Elastic scattering of electrons from chloroform

B. A. Hlousek ⬤, M. F. Martin, and M. A. Khakoo ⬤[*]

Department of Physics, California State University, Fullerton, California 92834, USA

M. Zawadzki ⬤

Department of Physics, California State University, Fullerton, California 92834, USA
and Atomic Physics Division, Department of Atomic, Molecular and Optical Physics, Faculty of Applied Physics and Mathematics,
Gdańsk University of Technology, ul. G. Narutowicza 11/12, 80-233 Gdańsk, Poland

G. M. Moreira, L. S. Maioli, and M. H. F. Bettega[†]

Departamento de Física, Universidade Federal do Paraná, Caixa Postal 19044, 81531-990 Curitiba, Paraná, Brazil

L. E. Machado

Departamento de Física, Universidade Federal de São Carlos, 13565-905 São Carlos, São Paulo, Brazil

V. A. S. da Mata, A. J. da Silva, I. Iga, M.-T. Lee, and M. G. P. Homem ⬤[‡]

Departamento de Química, Universidade Federal de São Carlos, 13565-905 São Carlos, São Paulo, Brazil

We present experimental and theoretical cross sections for elastic electron scattering from CHCl$_3$. This is an important target because of its relevance to environmental chemistry and the plasma etching industry as a source of chlorine radicals. The experimental results were obtained at incident electron energies ranging from 0.5 to 800 eV in the $10°$–$130°$ scattering angle range. Theoretically, the scattering cross sections in the low-energy region were obtained by using the Schwinger multichannel method with pseudopotentials in the static-exchange plus polarization approximation. Additionally, in the low- and intermediate-energy ranges, theoretical calculations were also performed using a molecular complex optical potential and a single-center expansion method combined with Padé approximation. Further calculations using the independent atom model were also made at intermediate energies. Momentum-transfer cross sections were derived by integrating the differential cross sections. In general, there is a good agreement between the experimental data and the theoretical results. Moreover, the calculations reveal the presence of three shape resonances in the elastic channel, located at 0.5, 2, and 8 eV. The two higher-lying resonances were confirmed by the present experiments, whereas the positions of the two lower-lying resonances agree well with previous results of electron attachment experiments.

I. INTRODUCTION

The study of electron scattering from chlorine-containing compounds has important applications in that the electron impact of such compounds is significant in etching processes as a source of chlorine atoms [1–4]. Such compounds are also frequently used in organic chemistry as both reactants and solvents. As a result of these applications, there is an expected increase in the concentration of chlorine-containing molecules in the atmosphere which has environmental consequences. Many such chlorine compounds have long atmospheric lifetimes and may stay in the earth's troposphere for several decades [4]. There they may interact with UV radiation, resulting in the formation of neutral and ionized species such

as free chlorine radicals, which are known to act as catalysts in chain reactions with ozone. In fact, a recent study indicated [5] that the concentration of chloromethanes (CH$_n$Cl$_{4-n}$) has increased in the atmosphere and may contribute to an increased loss of ozone in the lower stratosphere.

The development of new technologies to reduce the emission of such compounds into the atmosphere are therefore of sufficient interest. For example, nonthermal plasma processing (NPP) has been used as a modern and efficient technique to eliminate small concentrations of volatile organic compounds from industrial waste-gas streams [6]. Compared to other established technologies such as catalytic oxidation, thermal decomposition, etc., NPP is better suited to remove chlorinated compounds, particularly those difficult to decompose [7–9]. It is expected that the electron-collision cross sections of chlorine-substituted methanes would be important to shed light on the underlying physics of such processes since they are necessary for the determination of reaction rates [2,3,10].

---
[*]mkhakoo@fullerton.edu
[†]bettega@fisica.ufpr.br
[‡]mghomem@ufscar.br

Presently, the existing experimental results of electron-scattering cross sections for the family of chloromethanes (CH_nCl_{4-n}) include those of chloromethane (CH_3Cl) [11–14], carbon tetrachloride (CCl_4) [15,16], and very recently dichloromethane (CH_2Cl_2) [17,18]. On the other hand, although chloroform ($CHCl_3$) is a major industrial reactant and solvent, there are only comprehensive experimental data of dissociative electron attachment (DEA) processes in the low-energy region for this molecule. Such investigations include the works of Scheunemann *et al.* [19], Matejčík *et al.* [20,21], Aflatooni *et al.* [22], Denifl *et al.* [23], and Kopyra *et al.* [24] using the mass spectroscopy technique, and those of Guerra *et al.* [25] and Aflatooni *et al.* [26] using the electron transmission technique. However, there are no experimental electron-scattering cross-section data for chloroform except the grand-total cross section reported by Karwasz *et al.* [14]. Also, differential cross sections (DCSs) for electron scattering by chloroform at energies up to 30 eV were only reported by Natalense *et al.* [27] using the Schwinger multichannel (SMC) method.

In this work we report a joint experimental and theoretical study of vibrationally summed elastic electron scattering from $CHCl_3$. The low-energy DCS measurements covered in the incident electron energy (E_0) range of 0.5–30 eV were carried out by the California State University, Fullerton (CSUF) group, and the intermediate-energy DCS measurements in the 20–800 eV range were performed by the Universidade Federal de São Carlos (UFSCar) group. The experimental measurements were deemed vibrationally summed elastic because the experimental setups in UFSCar do not resolve vibrational modes with energy-loss values $\leqslant 0.5$ eV. The energy resolution of the experimental setup in CSUF is around 0.05 eV. Therefore, all the vibrational modes except the *d*-deformation mode at 0.032 eV energy losses [28,29] were resolved and their contributions were not accounted. Thus, their measured DCSs are a sum of the contributions of vibrationally elastic and vibrational excitation of the *d*-deformation mode. The experimental DCSs of the CSUF group were obtained at E_0 values of 0.5, 1, 2, 3, 4, 5, 7, 10, 15, 20, and 30 eV, and those of the UFSCar group are values of 20, 30, 50, 100, 150, 200, 300, 400, 500, and 800 eV, in both cases for scattering angles (θ) from 10° to 130°. The absolute values of DCSs are determined using the relative flow technique (RFT) [30]. The CSUF group has used He as the secondary standard, whereas Ar and N_2 were used as secondary standards in UFSCar.

In principle, one might derive the experimental integral (ICSs) and momentum-transfer (MTCSs) cross sections via numerical integration of measured DCSs. For this purpose, the DCSs in the angular regions not covered in experiments are usually estimated via extrapolation. Nevertheless, this procedure is quite arbitrary, particularly at the scattering angles near the forward direction for strongly polar molecules due to the steep variation of the DCSs in that region, which may cause significant errors in the extrapolated data. On the other hand, theoretical treatments based on the Born approximation and the point-dipole description lead DCSs of electron scattering by polar symmetric-top molecules, like $CHCl_3$, to diverge in the forward direction, resulting in infinitely large ICSs, as pointed out by Crawford [31]. Although such divergent behavior can be avoided by use of rotational excitation from

the $J = 0$ state with rotational excitation energy taken appropriately into account, the direct comparison of experimental ICSs (generated using the extrapolated DCSs) and theoretical results is meaningless. It is mainly due to the fact that the DCSs which most contribute to the ICSs are not measured experimentally but estimated via extrapolation. In view of such difficulties, Fabrikant [32] pointed out alternatives to compare theoretical and experimental ICSs as follows:

(1) Compare partly integrated cross sections which includes scattering angles $\theta > \theta_0$ where the angle θ_0 is defined by the experimental geometry.

(2) Modify the experimentally measured cross sections by adding the low-angle contribution in the Born approximation.

(3) Abandon the comparison of the integrated cross sections and compare only differential.

According to him [32], the third option seems to be most appropriate. In view of this, we decided to not report ICSs but only the MTCSs in this work. In fact, the MTCSs are less affected by the uncertainties generated in the extrapolation procedures and are very important in the plasma modeling processes.

In the present work, theoretical DCSs and MTCSs were obtained by the Universidade Federal do Paraná (UFPR) group using the Schwinger multichannel method with pseudopotentials (SMCPP) in the static-exchange plus polarization (SEP) approximation in the 0.5–30 eV energy range. Additionally, at energies ranging from 0.5 to 150 eV, theoretical calculations were performed by the UFSCar group using a molecular complex optical potential (MCOP). A single-center expansion technique combined with Padé approximation was used to solve the scattering equations. Further calculations of cross sections were also made in UFSCar at 50 eV and above using the independent atom model (IAM) in which the atomic complex optical potential and partial-wave method were applied to obtain atomic scattering amplitudes. All the calculations were performed in a fixed-nuclei framework, i.e., the degrees of freedom of nuclear motions were not considered. Essentially, the DCSs calculated using this framework are vibrationally unresolved.

The organization of this paper is as follows: In Sec. II, we describe the experimental procedures. In Sec. III, the theory and details of the calculations are presented. In Sec. IV, we compare the present experimental and theoretical results, and in Sec. V, concluding remarks are presented.

II. EXPERIMENTAL PROCEDURES

A. Low-energy CSUF experiment

The CSUF experimental setup was detailed in, e.g., Khakoo *et al.* [33], so only a brief description is given here. We used a well-tested electron spectrometer in which both the electron gun and detector employed have double hemispherical energy selectors made of titanium. Cylindrical lenses transported electrons through the spectrometer, which was baked to about 80 °C–130 °C with magnetically free biaxial heaters [34] to maintain stability of the surfaces in the experiment to a period longer than 4 months of continuous operation. Electrons were detected by a discrete dynode electron multiplier [35] with a dark count rate of <0.01 Hz and

capable of linearly detecting $> 10^5$ Hz without saturating. The remnant magnetic field was reduced to ~ 1 mG at the collision region by a double μ-metal shield. Typical electron currents were around 18–25 nA, with an energy resolution of between 40 and 70 meV FWHM, which was mostly dependent on tuning of the spectrometer rather than the current the gun outputted. Lower currents were chosen for lower E_0 values to minimize the space-charge broadening of the incident electron beam. The electron beam could be focused at 0.5 eV and remained stable, varying less than 15% at maximum during the data acquisition period. The energy of the beam was established by measuring the minimum in the elastic scattering of the $2^2 S$ He resonance at 19.366 eV [36] at a θ of 90° to ~ 40 meV stability during a daily run. Typically the contact potential varied between 0.55 and 0.65 eV. The elastic peaks of the energy-loss spectra were collected at fixed E_0 and θ values by repetitive multichannel-scaling techniques. The effusive target gas beam was formed by flowing gas through a ~ 0.4-mm-diameter aperture, which was sooted (using an acetylene flame) to reduce secondary electrons. In using the aperture source instead of a conventional tube gas collimator, we obviated the experimental need to maintain the backing pressures of the target gases in an inverse ratio of their molecular diameters (in order to equalize the mean-free path of the two target gases [37] in the gas collimating structure), thus removing an additional systematic source of error that could occur in using a conventional tube collimator or similar setups, see, e.g., [37]. This is a great advantage when working with heavy molecular targets of masses around 100 amu, since the uncertainty in the molecular diameters of such targets can be considerable, and applying the inverse molecular diameter gas pressure ratio accurately in the RFT at moderate or high target source pressures is made more challenging with controlling the stability in the flow of these viscous mass targets through collimating needle sources. The aperture, located ~ 7 mm below the axis of the electron beam, was incorporated into a movable source [37,38] arrangement which moved the aperture in alignment (signal $+$ background scattering) and out of alignment (background scattering) with the incident electron beam. The movable gas source method determined background electron-gas scattering rates expediently and accurately [37]. The measured DCSs were normalized using the RFT with helium as the reference gas, using DCSs from the well-established work of Nesbet [39] for $E_0 < 20$ eV and of Register *et al.* [40] for $E_0 \geqslant 20$ eV. The pressures behind the aperture ranged from 1.2 to 1.8 Torr for He and 0.06 to 0.13 Torr for $CHCl_3$, resulting in a chamber pressure ranging from 8×10^{-7} Torr to 1.8×10^{-6} Torr. The $CHCl_3$ liquid was obtained from Sigma-Aldrich and was $\geqslant 99.8\%$ purity. The liquid was placed in a 50-cm^3, all glass-metal flask attached by baked 1/4-inch refrigeration copper tubing to the experimental gas handling system (also continuously heated 1/4-inch refrigeration copper tubing), and the liquid sample was purified from dissolved gases in it by liquid N_2 freeze-pump cycles. $CHCl_3$ has a large molecular mass (119.38 amu), but it is not the heaviest target used in our system. Its raised viscosity caused periodic instabilities in the flow as it partly choked up our gas metering valve (Granville-Phillips Series 203 valve [41]). Therefore this valve was

baked at a temperature of about ~ 70 °C, which alleviated this problem. Also, the entire gas line after the metering valves was heated to ~ 95 °C to prevent condensation of $CHCl_3$ in the valve and gas lines. Each DCS was taken a minimum of two times to check its reproducibility, and weighted averaging was made of multiple data sets to obtain the final DCS.

B. Intermediate-energy UFSCar experiment

Two experimental setups were used in UFSCar to obtain the DCSs of $CHCl_3$. In the measurements at 100 eV and above, the setup already described in detail in several works, e.g., Hlousek *et al.* [18], as well as the same procedures and methodology were employed. In summary, a crossed electron beam–molecular beam geometry was used. The molecular beam was collimated by a thin molybdenum tube with a diameter-to-length aspect ratio of 0.03. The nonmonochromated electron beam with a typical energy resolution (ΔE) of 0.5 eV FWHM provides currents in the range of 50–150 nA. A retarding-field analyzer located in front of the detector limits the detection of only elastically scattered electrons within an energy window of about 1.5 eV. The measurements were performed in the angular range of 10°–130°.

The measurements at 20, 30, and 50 eV were performed using a new electron spectrometer, recently commissioned in the UFSCar Laboratory. The crossed-beam geometry was similarly used in this apparatus to define the collision region, and the molecular beam was generated by a molybdenum tube with an aspect ratio of 0.03. Nevertheless, the electron beam is generated by a commercial monochromatized electron source (Comstock EG-451) that employs a spherical sector electrostatic energy analyzer with a mean radius of 36.5 mm, and with an entrance and exit apertures of 1.0 and 0.5 mm diameter, respectively. A two-stage electrostatic lens positioned after the exit aperture of the spherical sector allowed us to vary the energy of the output electrons from a few eV to 1 keV. After the collision region, the scattered electrons transited through a three-element cylindrical lens with an entrance aperture diameter of 0.55 mm and then energy analyzed by a spherical sector analyzer of the same size of the former and detected by a microchannel plate. The analyzer can be rotated from $-10°$ to $110°$ with respect to the incident beam. All surfaces directly exposed to the electron-beam path are treated with colloidal graphite in order to reduce secondary scattering and also to homogenize surface potentials. A high-permeability magnetic shield (μ-metal) that covers the inner wall of the vacuum chamber reduced the magnetic fields to < 3 mG. Besides, both the electron monochromator and the analyzer systems are located inside of μ-metal boxes. The ΔE in this system is ~ 180 meV (FWHM at the elastic peak).

In both spectrometers, the base pressure was $\approx 1 \times 10^{-7}$ Torr and the working pressures were in the range of ≈ 1–3×10^{-6} Torr. The gaseous sample was obtained from the saturated vapor above the $CHCl_3$ liquid ($\geqslant 99.8\%$ purity) in a small vial attached to the gas handling system [42]. Several cycles of freeze-pump-thaw degassing were performed in order to eliminate atmospheric air and other volatile contaminants. Periodically during the experiment, the presence of

contaminants was checked using a quadrupole mass analyzer and was found to be negligible.

The angular distributions of the scattered electrons were converted to absolute DCSs using the RFT [30]. At 20 and 30 eV, the experimental elastic DCSs of N_2 reported by Shyn and Carignan [43] were used to normalize our data. At 50 and 800 eV, the absolute DCSs of DuBois and Rudd [44], and in the 100–500 eV range the DCSs reported by Jansen *et al.* [45] for electron scattering by Ar were used as references. For each E_0, the (relative) angular distribution of the scattered electrons was measured at least three times to verify its reproducibility, and the RFT normalization procedure was applied at least twice to place the angular distribution on absolute scale. Considering the reported uncertainties for the reference gases and the associated uncertainties of our experimental procedure, the estimated standard deviations in the DCSs are 17% at 20 eV, 30 eV, and 800 eV, 21% at 50 eV, and 11% at other energies.

The experimental MTCSs were obtained by numerical integration of DCSs. In the angular regions not covered by the experiment, values of DCSs were obtained by extrapolation following the procedure previously described [46,47]. Basically, the extrapolated data were obtained following the shape of the theoretical curves, except in the $0°$–$2°$ interval, where the trend of the extrapolated data for angles above $2°$ was used. Due to the difficulty involved in this procedure, particularly at small scattering angles, an extra error of about 20% was added in quadrature to the average error of the experimental data to estimate the overall error of the MTCSs [47].

III. THEORY AND NUMERICAL PROCEDURE

A. Schwinger multichannel method

The calculations at low energies were carried out using the SMCPP. The details of the method are published elsewhere [48,49], and here we will only discuss the theoretical aspects related to the present calculations.

The target ground state was described in the Hartree-Fock approximation at the experimental equilibrium geometry [50]. Since the SMC method deals with Abelian groups, our scattering calculations were carried out within the C_s symmetry group.

We used the norm-conserving pseudopotentials of Bachelet *et al.* [51] to replace the core electrons of the carbon and chlorine atoms. The one-particle basis set employed in both bound-state and scattering calculations has $6s5p2d$ uncontracted functions for each heavy atom with exponents, as shown in Table I, generated according to Ref. [52].

For the hydrogens, we employed the $4s/3s$ basis set of Dunning [53] augmented with one p-type function with exponent 0.75. In order to avoid linear dependency in the basis set, the symmetric combinations of the d-type orbital, namely, $[(x^2 + y^2 + z^2)\exp(-\alpha r^2)]$, were excluded from our calculations. The basis set of the $(N+1)$-electron system, known as configuration state functions (CSFs), is built from products of target states with single-particle functions. The scattering cross sections were computed in the SEP approximations. In the simplest approximation, namely, the static-exchange (SE) approximation, the polarization effects of the electronic

TABLE I. Exponents of the uncontracted Cartesian Gaussian functions used for carbon and chlorine.

Type	C	Cl
s	12.49408	10.49065
s	2.470291	6.836599
s	0.614027	2.420592
s	0.184029	0.513579
s	0.036799	0.188863
s	0.013682	0.062954
p	5.228869	6.037205
p	1.592058	2.012401
p	0.568612	0.686842
p	0.210326	0.218056
p	0.072250	0.071193
d	0.603592	1.611766
d	0.156753	0.328314

cloud are neglected. The $(N+1)$-electron basis set is given by a direct product between the target ground state, which is described in the Hartree-Fock level, and a single-particle function. On the other hand, the SEP approximation takes into account the polarization effects of the electronic cloud. At this level of approximation, the CSF space is augmented by considering direct products of N-electron states obtained by performing single (virtual) excitations of the molecular target from the occupied (hole) orbitals to a set of unoccupied (particle) orbitals and a single-particle function. We use the improved virtual orbitals (IVOs) [54] to represent the particle and scattering orbitals in the SEP calculations. We selected IVOs that satisfy the relation

$$\varepsilon_{par} - \varepsilon_{hole} + \varepsilon_{scat} < \Delta, \qquad (1)$$

where ε_{par} is the particle orbital energy, ε_{hole} is the hole orbital energy, ε_{scat} is the scattering orbital energy, and Δ is the energy cutoff. We used $\Delta = 2.17$ hartree and considered singlet- and triplet-coupled excitations for the A$'$ and A$''$ symmetries such that we employed 10 454 and 10 429 CSFs for the A$'$ and A$''$ symmetries, respectively.

In our calculation, the obtained value for the dipole moment was 1.01 D, which is about 3% less than the experimental value of 1.04 D [55]. In order to consider the permanent dipole effects, we used the Born-closure procedure [56]. This correction accounted for the scattering of higher partial waves due to the long-range character of the dipole potential. The SMC method employs only square integrable functions in the expansion of the scattering wave function, and as a consequence, the higher partial waves are not correctly described. Then, the Born-closure corrected scattering amplitude includes now a term for the dipole potential obtained within the first Born approximation (f^B) and takes the following expression:

$$f(\vec{k}_f, \vec{k}_i) = f^B(\vec{k}_f, \vec{k}_i) + \sum_{l=0}^{l_{SMC}} \sum_{m=-l}^{l}$$
$$\times [f_{lm}^{SMC}(k_f, \vec{k}_i) - f_{lm}^B(k_f, \vec{k}_i)]Y_{lm}(\hat{k}_f), \quad (2)$$

where the amplitude f_{lm}^B is obtained from an outgoing angular expansion of the first Born approximation scattering

amplitude in spherical harmonics, and f_{lm}^{SMC} is given from a similar expansion of the SMCPP scattering amplitude. As a result, the lower partial-wave ($l \leqslant l_{SMC}$) contributions are obtained by the SMCPP method, while the higher partial waves ($l > l_{SMC}$) are described with the first Born approximation for the dipole moment potential. The values of l_{SMC} are chosen to minimize the difference between the differential cross sections calculated with and without the Born-closure correction for scattering angles above $\sim 30°$. To overcome the divergence of the forward scattering amplitude, we employed an approximation to account for the inelastic $J = 0 \rightarrow J' = 1$ dipole allowed rotational excitation of a symmetric top [57] by making $k_f^2 = k_i^2 + 2\Delta E_{rot}$, where we used $\Delta E_{rot} \simeq [J'(J' + 1) - J(J + 1)]B_\perp = 2B_\perp$, with $\Delta E_{rot} = 7.257 \times 10^{-6}$ eV.

B. Molecular complex optical potential approximation

The elastic electron scattering by $CHCl_3$ was also studied by using the MCOP at the static-exchange polarization plus absorption (SEPA) level of approximation. In this approach, the many-body nature of the electron-molecule interaction was reduced to a one-particle scattering problem, and a single-center expansion combined with the [N/N] Padé approximation was used to solve the scattering equations, as described by Gianturco *et al.* [58] and Natalense and Lucchese [59]. The details of the methodology used in the present work has previously been described [60–63]. The static-exchange potential was derived from a near-Hartree-Fock self-consistent-field (HF-SCF) wave function of the target, whereas the correlation-polarization potential was obtained within the framework of the free-electron-gas model, derived from a parameter-free local density approach [64]. The absorption contribution was taken into account via the scaled quasifree scattering model (SQFSM) of Lee *et al.* [65], which is an improvement of the third version of the model absorption potential originally proposed by Staszewska *et al.* [66].

The HF-SCF wave function of $CHCl_3$ was obtained using the triple-zeta valence (TZV-3d) basis set of the Firefly QC package [67], which is partially based on the GAMESS (U.S.) [68] source code. The point group C_{3v} was used in our calculations to describe the symmetry of the molecule. For the experimental ground-state molecular geometry [50], this basis provided a total energy of –1416.9786 hartree. The calculated electric dipole moment was 1.26 D, about 17% larger than the experimental value of 1.04 D [55]. The asymptotic form of the correlation-polarization potential was generated using the calculated dipole polarizabilities [50] $\alpha_{xx} = 58.84$ a.u., $\alpha_{yy} = 58.84$ a.u., and $\alpha_{zz} = 42.34$ a.u. The value of α_0 is 53.34 a.u., about 17% lower than the experimental value of 64.2 a.u. [55].

In the present calculation, the target wave function and interaction potentials were partial-wave expanded about the center of mass of the molecule in terms of symmetry-adapted functions [69]. The truncation parameters used in these expansions were $l_c = 30$ for the bound orbitals and $l_c = 60$ for the interaction potentials. The cutoff parameter $l_c = 30$ was used for the continuum orbitals and for the T-matrix elements at 50 eV and above. At lower energies, $l_c = 20$ was used. The calculated cross sections were converged up to 10 iterations. Also, a rotating point-dipole Born-closure

formula was used to take into account the effects of higher partial-wave contributions to the scattering amplitudes. This procedure was the same as that used in some of our past works [62,70]. Briefly, the Born-closure corrected scattering amplitude in the body frame is written as [70]

$$f(\vec{k}_f, \vec{k}_i) = f^B(\vec{k}_f, \vec{k}_i) + \frac{1}{k} \sum_{p\mu lhl'h'}^{LL'} i^{l-l'} \left(f_{klhl'h'}^{p\mu} - f_{klhl'h'}^{B,p\mu} \right)$$
$$\times X_{lh}^{p\mu}(\hat{k}_f) X_{l'h'}^{p\mu*}(\hat{k}_i), \qquad (3)$$

where f^B and $f_{klhl'h'}^{B,p\mu}$ are the total and partial-wave expansion scattering amplitudes in the first Born approximation (FBA), respectively, both calculated using the point-dipole potential, and $X_{lh}^{p\mu}$ are symmetry-adapted functions [69]. It is known that f^B for elastic scattering of a charged particle by a point-dipole potential diverge in the forward direction [31,32]. In order to avoid this divergent behavior, we made use of an approximation described as follows. First, a body-frame to laboratory (Lab)-frame transformation was performed on Eq. (3). Then the Lab-frame elastic FBA scattering amplitude is replaced by the $J = 0 \rightarrow J' = 1$ rotational excitation inelastic scattering amplitude of a symmetric-top rotor [31]. Using this approximation, the elastic momentum-transfer vector $\vec{q}$ which vanishes at zero scattering angle, leading to divergent DCS, is replaced by a rotational inelastic momentum-transfer vector whose magnitude is given as $q = k_i - k_f$ at $\theta = 0°$. Since $k_f^2 = k_i^2 + 2\Delta E_{rot}$ and ΔE_{rot} is the rotational excitation energy, q would not vanish in the forward direction, which results in a very large but finite DCS at the zero scattering angle.

C. Independent atom model

For 50 eV and above, DCSs were also calculated in the IAM framework at the SEPA level of approximation. The procedure and interaction potentials are detailed in our previous work [71]. In summary, the static atomic potentials reported by Salvat *et al.* [72] and the exchange potential proposed by Furness and McCarthy [73] were used. The model potential of Perdew and Zunger [64] and the SQFSM potential of Lee *et al.* [65] were used to account for the correlation-polarization and the absorption contributions, respectively. The atomic polarizabilities, the internuclear distances, and the mean excitation energy (considered as the first ionization potential) used in the calculations were taken from the literature [55]. Additionally, the MTCSs were obtained using the IAM additivity rule (AR) [74].

IV. RESULTS AND DISCUSSION

The experimental DCSs and MTCSs for elastic electron scattering by $CHCl_3$ obtained in CSUF and UFSCar are listed in Tables II and III, respectively. A comparison of these DCSs with the present theoretical results, calculated with the SMCPP, MCOP, and IAM methods, is shown in Figs. 1, 2, and 3.

In Fig. 1 we show the DCSs measured by the CSUF group at energies of 0.5, 1, 3, and 5 eV in comparison with the theoretical data calculated using the SMCPP and the MCOP approaches. Both calculations were performed at the SEP

TABLE II. Experimental DCSs (in 10^{-16} cm^2/sr) and MTCSs (in 10^{-16} cm^2) from the CSUF experiment for elastic electron scattering from CHCl$_3$. The average DCSs standard deviations are 13%. The estimated standard deviations of the MTCSs are around 20%.

Angle (deg)	E_0 (eV)										
	0.5	1.0	2.0	3.0	4.0	5.0	7.0	10.0	15.0	20.0	30.0
10									52.4	45.9	56.6
15					10.6	16.1	18.1	40.5	38.1	29.0	26.9
20		16.6	12.7	12.5	7.59	11.6	13.0	23.5	25.9	18.7	11.3
25		11.3	10.6	10.2	6.54	8.02	8.69	15.7	16.5	10.3	4.98
30	16.4	7.32	7.79	8.38	5.64	5.99	6.41	8.83	8.01	5.36	2.78
40	12.8	4.12	5.52	6.72	4.13	4.43	3.11	3.11	2.86	3.15	2.64
50	8.89	2.74	4.38	5.48	3.39	3.09	1.89	2.39	3.15	2.10	1.47
60	7.73	2.39	3.82	4.21	2.53	2.34	1.47	2.53	2.78	1.55	0.448
70	7.23	2.47	3.56	3.57	1.91	2.13	1.53	2.53	1.59	0.939	0.391
80	7.48	2.88	3.57	3.17	1.82	1.98	1.93	2.28	1.18	0.706	0.449
90	7.03	2.81	3.75	2.91	1.89	2.01	2.08	2.19	1.27	0.869	0.670
100	8.07	2.93	3.44	2.64	1.47	1.76	1.90	1.65	1.31	0.901	0.708
110	9.38	3.02	3.23	2.46	1.68	1.71	1.61	1.56	1.16	0.867	0.662
120	9.80	3.24	3.44	2.12	1.48	1.47	1.39	1.72	1.10	0.921	0.446
130	12.5	3.76	3.53	2.04	1.20	1.39	1.56	2.08	1.06	0.744	0.285
MTCS	153	49.6	47.0	32.8	19.5	21.3	23.0	30.6	17.2	11.4	6.52

level of approximation. At 0.5 and 1 eV, some unphysical oscillations appeared in the calculated MCOP DCSs which were caused by the poor convergence of the scattering wave functions, likely due to the slow fall-off of the long-range potentials of dipole and quadrupole natures. The Born-closure procedure based on the rotating point-dipole model was unable to eliminate such oscillations and therefore, a smoothing procedure was applied to the MCOP DCS curves at these energies.

As already mentioned, the experimental data of CSUF contain partial contributions from vibrational excitation. The contributions of the vibrationally resolved modes (not accounted for in the present results) vary from 5% to 7% at small scattering angles to about 20% at large angles, which seems to be roughly independent of the incident energies. On the other hand, the theoretical results are vibrationally unresolved, that is, they are a sum of all vibrational elastic and inelastic DCSs and thus are expected to be 5% to 20% larger. At 0.5 eV, the SMCPP calculation reproduced very well the shape of the experimental data but systematically underestimated their magnitudes. The MCOP calculation also reproduces reasonably the shape of the experimental data. Quantitatively, the MCOP calculation agrees well with the experiment at angles up to 60° but underestimates the DCSs at larger angles. At 1 eV, the SMCPP calculation still underestimates the experiment,

TABLE III. Experimental DCSs (in 10^{-16} cm^2/sr) and MTCSs (in 10^{-16} cm^2) from the UFSCar experiment for elastic electron scattering from CHCl$_3$. The average DCSs standard deviations are 17%. The estimated standard deviations of the MTCSs are around 30%.

| Angle (deg)	E_0 (eV)									
	20	30	50	100	150	200	300	400	500	800
10			39.4	8.12	6.55	4.90	3.74	2.82	2.69	2.88
15			14.1	4.32	3.46	2.98	1.71	1.62	1.67	1.17
20		17.8	5.10	2.33	1.76	1.50	1.25	1.22	0.896	0.739
25	8.59	6.65	2.89	1.32	0.962	1.17	0.816	0.610	0.531	0.459
30	3.96	4.28	2.32	0.952	0.810	0.885	0.451	0.44	0.386	0.313
35	3.16	4.08	1.80							
40	3.20	3.62	1.20	0.510	0.568	0.571	0.355	0.353	0.275	0.194
50	2.76	1.59	0.39	0.279	0.284	0.333	0.241	0.201	0.149	0.103
60	1.35	0.587	0.23	0.194	0.226	0.241	0.162	0.113	0.084	0.063
70	0.634	0.411	0.29	0.173	0.179	0.156	0.137	0.073	0.059	0.044
80	0.801	0.573	0.46	0.179	0.148	0.107	0.064	0.055	0.041	0.031
90	0.900	0.764	0.56	0.134	0.092	0.056	0.045	0.038	0.034	0.028
100	0.974	0.858	0.54	0.088	0.050	0.030	0.039	0.039	0.033	0.025
110	0.995	0.667	0.46	0.047	0.028	0.025	0.043	0.042	0.034	0.024
120				0.035	0.039	0.034	0.061	0.051	0.039	0.024
130				0.070	0.075	0.068	0.083	0.060	0.044	0.023
MTCS	13.6	7.29	5.10	3.01	2.23	1.63	1.35	0.992	0.744	0.478
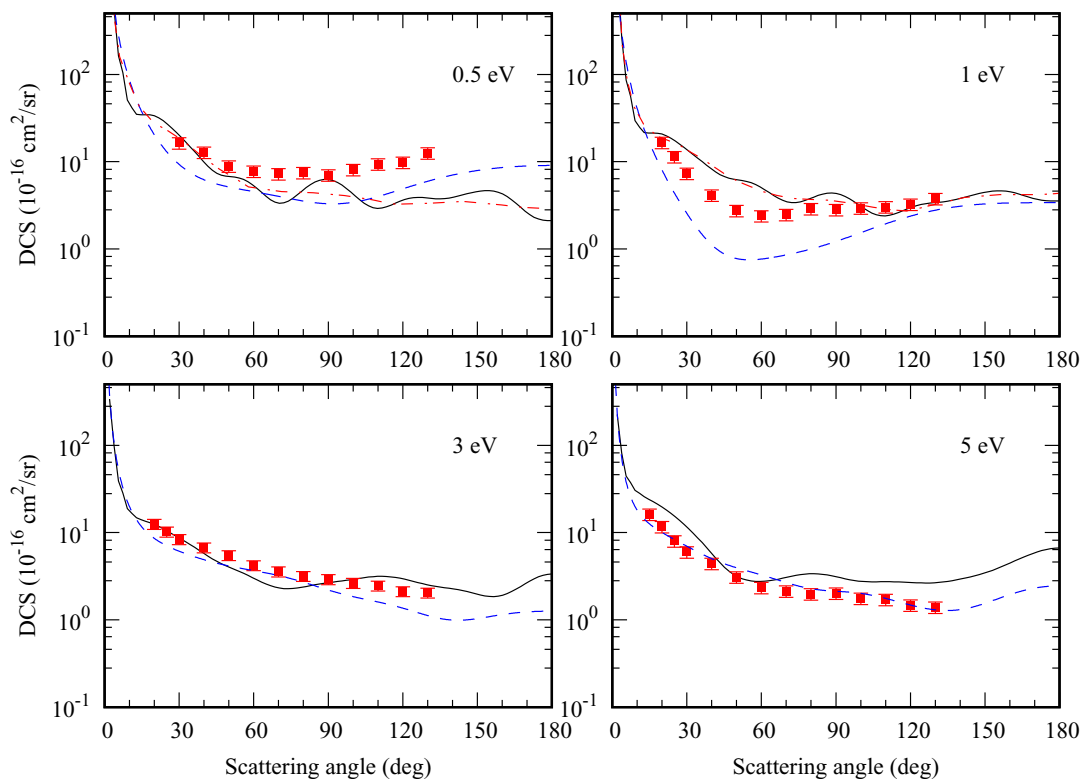
FIG. 1. DCSs for elastic scattering from $CHCl_3$ at $E_0 = 0.5$, 1.0, 3.0, and 5.0 eV. Experiment: (●) CSUF data. Theory: (- - -) SMCPP SEP calculation; (—) MCOP SEP calculation; (–·–·–) smoothed MCOP SEP data.
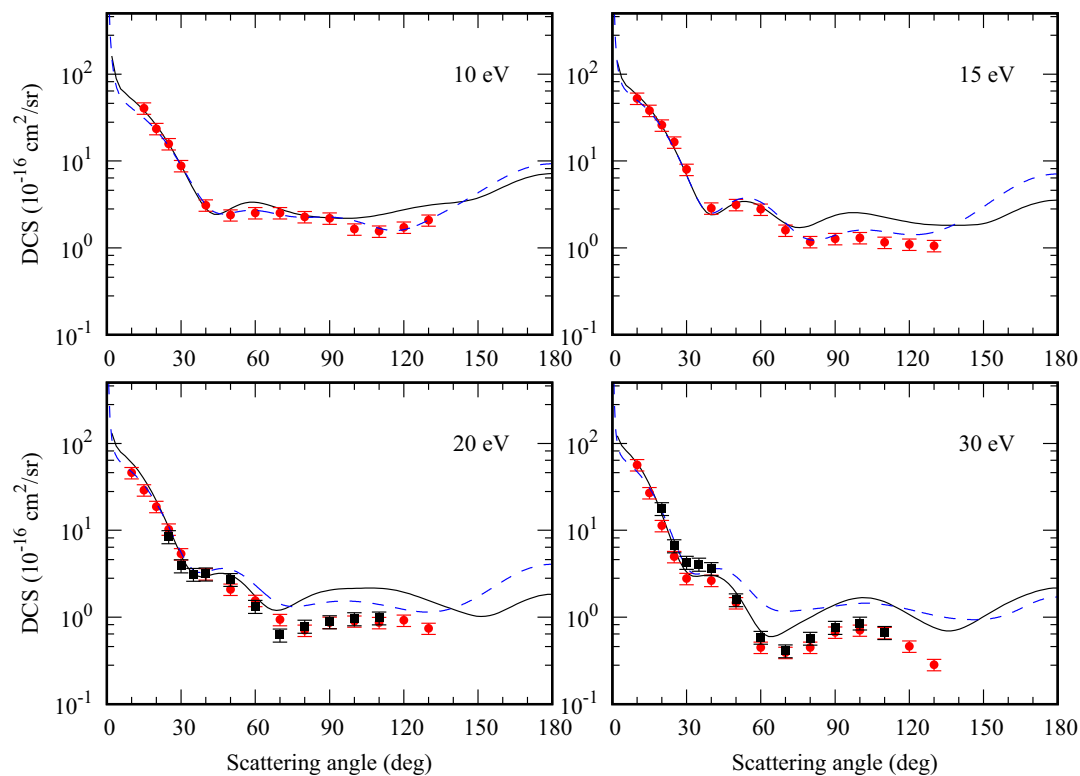

FIG. 2. DCSs for elastic scattering from $CHCl_3$ at $E_0 = 10$, 15, 20, and 30 eV. Experiment: (●) CSUF data; (■) UFSCar data. Theory: (- - -) SMCPP SEP calculation; (—) MCOP SEPA calculation.
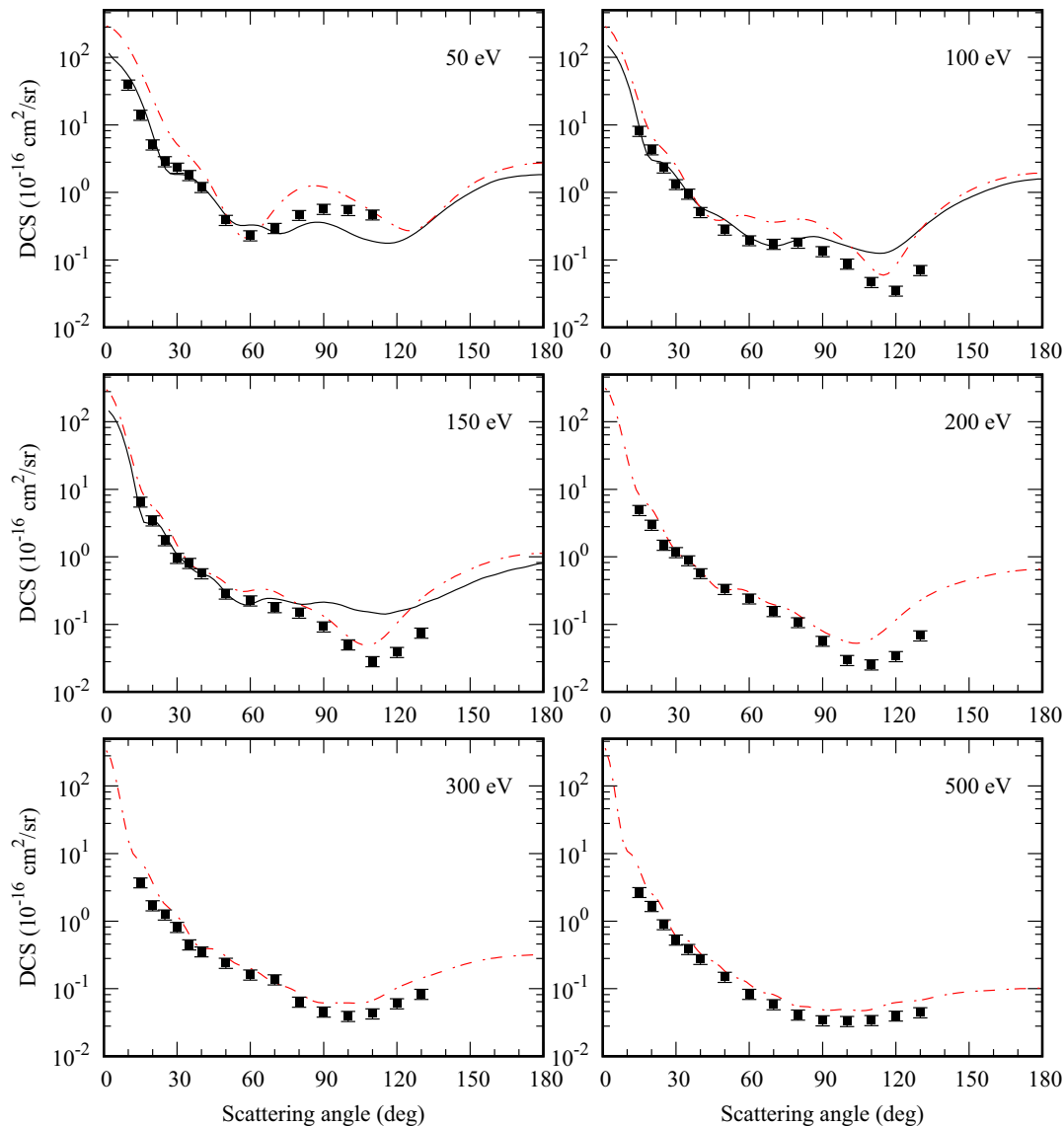
FIG. 3. DCSs for elastic scattering from $CHCl_3$ at $E_0 = 50$, 100, 150, 200, 300, and 500 eV. Experiment: (■) UFSCar data. Theory: (—) MCOP SEPA calculations; (– · – · –) IAM SEPA results.

whereas the calculated data with MCOP agree well with the experimental DCSs at small and large scattering angles. The agreement between theories and experiments significantly improves at higher energies. At 3 eV, the MCOP DCSs agree very well with the experimental data, although the SMCPP results disagree from the measured data at angles above 90°. In contrast, at 5 eV, excellent agreement is seen between the SMCPP calculation and experiments while the MCOP calculations overestimate the DCSs. At such low incident energies, the electron-scattering process is very sensitive to the action of long-range interaction potentials. Therefore, the details of the dynamics of interaction must be correctly represented in the calculations. Small failure in the description of such interactions can cause significant discrepancies as seen in the figures.

In Fig. 2 we compare the experimental results obtained by the CSUF group at 10-, 15-, 20-, and 30-eV incident energies with the calculated data using both the SMCPP and the MCOP. At 20 and 30 eV, the experimental data

obtained by the UFSCar group are also shown for comparison. It is seen that there is excellent agreement, both in shape and magnitude, between the measurements of the CSUF and UFSCar groups at these two energies. As mentioned above, the experimental data of the UFSCar group are completely vibrationally unresolved. Therefore, it is expected that the DCSs of the UFSCar group should be larger (around 5%–20%) than CSUF DCSs. This seems to be true in most of the data points. The comparison with the experiments shows that in general, both SMCPP and MCOP calculations are able to reproduce the shape of the experimental data very well. The quantitative agreement is also reasonable. At these energies, it is expected that the scattering electrons would penetrate more into the molecule and so their interaction with the bound electrons would be dominant. The satisfactory theory-experiment agreement reflects the good description of this dynamics in calculations.

In Fig. 3 we compare the experimental results obtained by the UFSCar group at energies ranging from 50 to 500 eV
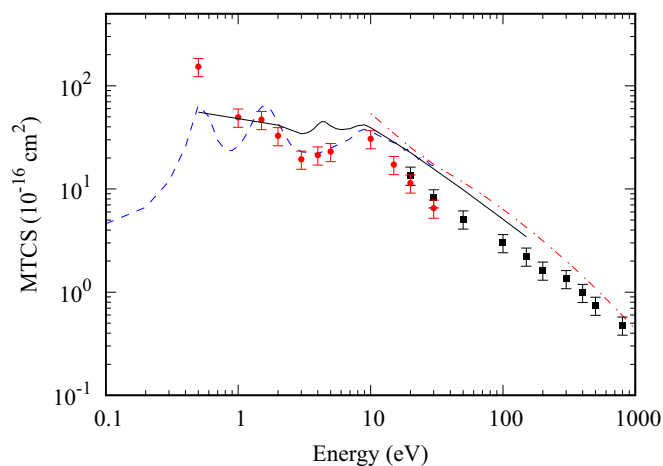
FIG. 4. MTCSs for elastic electron scattering from $CHCl_3$. Experiment: (●) CSUF data; (■) UFSCar data. Theory: (- - -) SMCPP SEP calculation; (—) MCOP SEPA calculation; (- · - ·) IAM-AR SEPA results.

FIG. 5. DCSs for elastic scattering from $CHCl_3$ at $\theta = 90°$. Experiment: (●) CSUF data; (■) UFSCar data; Theory: (- - -) SMCPP SEP calculation; (—) MCOP SEPA calculation.

with the calculated data using MCOP and IAM approaches. In the 50–150 eV range, there is a generally good agreement between the MCOP theory and experiments, particularly for scattering angles up to 80°. Nevertheless, the deep minimum located at about 110° shown in the experimental data at 100 and 150 eV is not reproduced by the MCOP calculations, which appears too shallow. Moreover, the results obtained by the IAM calculations in the 50–200 eV reproduce, quite well, the qualitative behavior of the measured data, but they lie generally above. At higher incident energies, there is a very good agreement between the IAM results and experimental DCSs. This good performance of the IAM calculations can be understood as follows. At incident energy of hundreds eV and above, the scattering electrons may penetrate deeply into the target so that the interactions with the atomic cores become dominant. Such interactions are treated exactly in the IAM due to its multicenter nature.

In Fig. 4 we present comparisons of the experimental MTCSs with the theoretical data calculated using the SMCPP, MCOP, and IAM-AR. It is seen that MTCSs calculated using the SMCPP exhibit three features: a sharp peak located at 0.5 eV, another peak at near 2 eV, and a broad enhancement centered near 8 eV. The peak at near 2 eV and the enhancement at 8 eV are confirmed by the experimental data of the CSUF group, which suggests the occurrence of shape resonances at these energies. On the other hand, the existence of the peak located at 0.5 eV is inconclusive in the present work, since there is no experimental data fully covering this region except for one point at 0.5 eV. The occurrence of the peak at near 2 eV and the enhancement at 8 eV can also be observed in the experimental fixed angle (90°) DCS results as a function of E_0, as shown in Fig. 5. The SMCPP calculations gave good descriptions of positions of the resonances. However, there are some structures above 10 eV in the SMCPP calculations, which are called pseudoresonances, and are due to the closed channels included in the polarization calculations that have the energy to be open [75]. In order to precisely locate the position of the resonances, we employed
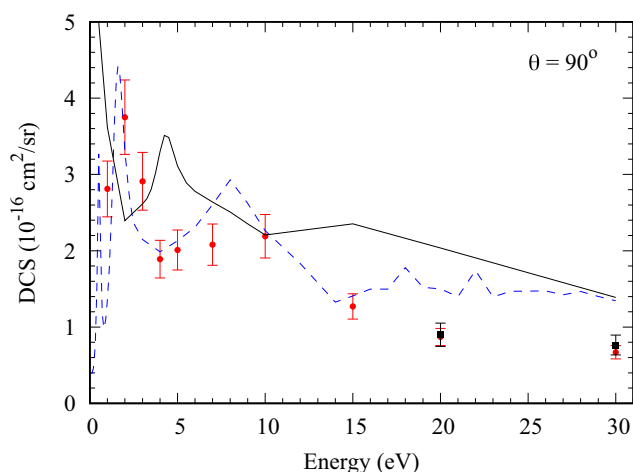
an empirical scaling relation proposed by Aflatooni et al. [76] that relates the virtual orbital energy (VOE) to the vertical attachment energy (VAE) through Koopmans' theorem. This relation is given by VAE = $0.90 \times$ VOE $- 2.55$ (both VAE and VOE in eV). To obtain the VOE, we perform electronic structure calculations. The ground-state geometry of $CHCl_3$ was optimized at the second-order Møller-Plesset perturbation theory (MP2) with the 6-31G(d) basis set using the GAMESS [68] computational package, and the VOE was obtained in a Hartree-Fock calculation at this optimized geometry and with the same basis. The values of the VAE corresponding to a_1 and e orbitals were 0.37 and 1.91 eV, respectively, which can be associated with the present experimental results at about 0.5 and 2 eV, in good agreement with the results of electron transmission experiments of Guerra et al. [25] (0.35 and 1.8 eV) and Aflatooni et al. [26] (0.42 and 1.8 eV). Moreover, the three lowest unoccupied molecular orbitals, shown in the Fig. 6, namely, LUMO, LUMO+1, and LUMO+2, which
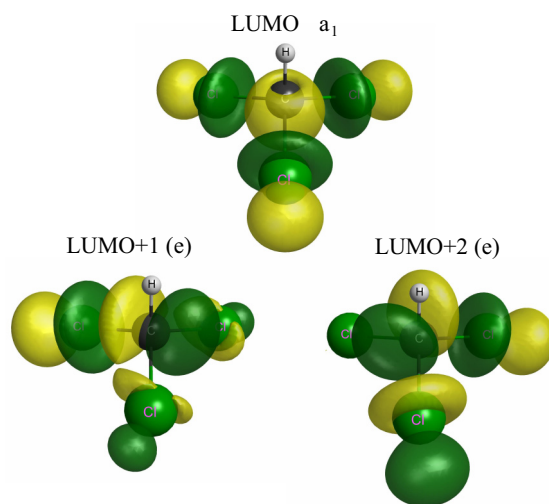

FIG. 6. Lowest unoccupied molecular orbital (LUMO) (a_1), LUMO+1 (e), and LUMO+2 (e) for $CHCl_3$.

belong to the A_1 and E symmetries of the C_{3v} point group, represent a good approximation of the resonant orbitals. In addition, the enhancement seen near 8 eV probably results from both the C-H ($k\sigma^*$) and the C-Cl ($k\sigma^*$) shape resonances [15]. It may also account for the contribution of a Rydberg resonance since it lies above the lowest electronic $n \rightarrow \sigma^*$ transition [77].

The MCOP results of MTCSs also show two resonancelike features: a peak at near 4 eV and a broad enhancement centered at 8 eV. The peak at 4 eV should correspond to that obtained by SMCPP at near 2 eV. The shift of the position to higher incident energies is due to the different treatments of polarization effects between the SMCPP and the MCOP. Apparently, the polarization contributions in the SMCPP calculations are stronger that pull the resonances to lower energies. In general, there is a good quantitative agreement between the experimental MTCSs with those calculated using the SMCPP and the MCOP. Nevertheless, the IAM-AR calculations systematically overestimate the experiment.

V. CONCLUSIONS

This study presents a joint theoretical-experimental investigation on electron collision with chloroform over a wide E_0 range. Experimental DCSs and MTCSs are reported in the $E_0 = 0.5$–800 eV range. The measurements at low E_0 (up to 30 eV) were carried out in CSUF and in the 20–800 eV performed in UFSCar. The reliability of our experimental data is supported by the good agreement between the measured DCSs of CSUF and UFSCar at overlapping energies of 20 and 30 eV using different experimental setups and procedures. Theoretical DCSs and MTCSs were also calculated using the SMCPP SEP in the 0.5–30 eV range, the MCOP SEPA in the

0.5–150 eV range, and with the standard IAM SEPA approach in the 50–800 eV range. The comparison between theories and experiments has shown that the SMCPP and MCOP calculations are able to reproduce quite well the experimental data for energies of 10 eV and above. The DCSs obtained by standard IAM calculations are also in good agreement with the experimental data at energies higher than 100 eV. Moreover, the SMCPP calculations have predicted the occurrence of three resonances centered at 0.5, 2, and 8 eV, respectively. The last two resonances were confirmed by present experiments. Finally, we expect that the present experimental DCSs, in wide ranges of E_0 and θ, could contribute to the efforts to provide collision data for modeling and furthering an understanding of the underlying physics in the various technological applications mentioned in the Introduction. We hope that the present study will stimulate further theoretical and experimental studies of this target.

[1] G. S. Oehrlein and S. Hamaguchi, Plasma Sources Sci. Technol. **27**, 023001 (2018).

[2] S. Huang and J. T. Gudmundsson, Plasma Sources Sci. Technol. **24**, 015003 (2014).

[3] E. Kemaneci, E. Carbone, J.-P. Booth, W. Graef, J. Van Dijk, and G. Kroesen, Plasma Sources Sci. Technol. **23**, 045002 (2014).

[4] V. M. Donnelly and A. Kornblit, J. Vac. Sci. Technol. A **31**, 050825 (2013).

[5] R. Hossaini, M. P. Chipperfield, S. A. Montzka, A. A. Leeson, S. S. Dhomse, and J. A. Pyle, Nat. Commun. **8**, 15962 (2017).

[6] T. J. Wallington, M. D. Hurley, and W. F. Schneider, Chem. Phys. Lett. **251**, 164 (1996).

[7] T. Zadi, A. A. Assadi, N. Nasrallah, R. Bouallouche, P. N. Tri, A. Bouzaza, M. M. Azizi, R. Maachi, and D. Wolbert, Chem. Eng. J. **349**, 276 (2018).

[8] R. Zhu, Y. Mao, L. Jiang, and J. Chen, Chem. Eng. J. **279**, 463 (2015).

[9] Z. Abd Allah, J. C. Whitehead, and P. Martin, Environ. Sci. Technol. **48**, 558 (2013).

[10] K. Bartschat and M. J. Kushner, Proc. Nat. Acad. Sci. USA **113**, 7026 (2016).

[11] X. Shi, V. K. Chan, G. A. Gallup, and P. D. Burrow, J. Chem. Phys. **104**, 1855 (1996).

[12] H. Kato, T. Asahina, H. Masui, M. Hoshino, H. Tanaka, H. Cho, O. Ingólfsson, F. Blanco, G. Garcia, S. J. Buckman, and M. J. Brunger, J. Chem. Phys. **132**, 074309 (2010).

[13] C. Navarro, A. Sakaamini, J. Cross, L. R. Hargreaves, M. A. Khakoo, K. Fedus, C. Winstead, and V. McKoy, J. Phys. B: At., Mol. Opt. Phys. **48**, 195202 (2015).

[14] G. P. Karwasz, R. S. Brusa, A. Piazza, and A. Zecca, Phys. Rev. A **59**, 1341 (1999).

[15] P. Limão Vieira, M. Horie, H. Kato, M. Hoshino, F. Blanco, G. García, S. J. Buckman, and H. Tanaka, J. Chem. Phys. **135**, 234309 (2011).

[16] A. Zecca, G. P. Karwasz, and R. S. Brusa, Phys. Rev. A **46**, 3877 (1992).

[17] K. Krupa, E. Lange, F. Blanco, A. S. Barbosa, D. F. Pastega, S. d'A. Sanchez, M. H. F. Bettega, G. García, P. Limão-Vieira, and F. Ferreira da Silva, Phys. Rev. A **97**, 042702 (2018).

[18] B. A. Hlousek, M. F. Martin, M. Zawadzki, M. A. Khakoo, L. E. Machado, R. R. Lucchese, V. A. S. da Mata, I. Iga, M.-T. Lee, and M. G. P. Homem, J. Phys. B: At., Mol. Opt. Phys. **52**, 025204 (2018).

[19] H.-U. Scheunemann, E. Illenberger, and H. Baumgärtel, Ber. Bunsen-Ges. **84**, 580 (1980).

[20] Š. Matejčík, G. Senn, P. Scheier, A. Kiendler, A. Stamatovic, and T. D. Märk, J. Chem. Phys. **107**, 8955 (1997).

[21] Š. Matejčík, V. Foltin, M. Stano, and J. D. Skalný, Int. J. Mass Spectrom. **223**, 9 (2003).

[22] K. Aflatooni, G. A. Gallup, and P. D. Burrow, J. Phys. Chem. A **104**, 7359 (2000).

[23] S. Denifl, A. Mauracher, P. Sulzer, A. Bacher, T. Märk, and P. Scheier, Int. J. Mass Spectrom. **265**, 139 (2007).

[24] J. Kopyra, I. Szamrej, K. Graupner, L. M. Graham, T. A. Field, P. Sulzer, S. Denifl, T. D. Märk, P. Scheier, I. I. Fabrikant, M. Braun, M.-W. Ruf, and H. Hotop, Int. J. Mass Spectrom. **277**, 130 (2008).

[25] M. Guerra, D. Jones, G. Distefano, F. Scagnolari, and A. Modelli, J. Chem. Phys. **94**, 484 (1991).

[26] K. Aflatooni and P. D. Burrow, J. Chem. Phys. **113**, 1455 (2000).

[27] A. P. P. Natalense, M. H. F. Bettega, L. G. Ferreira, and M. A. P. Lima, Phys. Rev. A **59**, 879 (1999).

[28] T. Shimanouchi, *Tables of Molecular Vibrational Frequencies Consolidated* (National Bureau of Standards, Gaithersburg, MD, 1972), Vol. 1, pp. 1–160.

[29] J. Morcillo, J. Biarge, J. Heredia, and A. Medina, J. Mol. Struct. **3**, 77 (1969).

[30] S. K. Srivastava, A. Chutjian, and S. Trajmar, J. Chem. Phys. **63**, 2659 (1975).

[31] O. H. Crawford, J. Chem. Phys. **47**, 1100 (1967).

[32] I. I. Fabrikant, J. Phys. B: At., Mol. Opt. Phys. **49**, 222005 (2016).

[33] M. A. Khakoo, C. E. Beckmann, S. Trajmar, and G. Csanak, J. Phys. B: At., Mol. Opt. Phys. **27**, 3159 (1994).

[34] ARi Industries Inc., Addison, IL 60101, USA, 1HN040B-16.3 biaxial cable.

[35] ETPEquipe Thermodynamique et Plasmas (ETP) model af151.

[36] J. N. H. Brunt, G. C. King, and F. H. Read, J. Phys. B **10**, 433 (1977).

[37] M. A. Khakoo, K. Keane, C. Campbell, N. Guzman, and K. Hazlett, J. Phys. B: At., Mol. Opt. Phys. **40**, 3601 (2007).

[38] M. Hughes, K. E. James, Jr., J. G. Childers, and M. A. Khakoo, Meas. Sci. Technol. **14**, 841 (2003).

[39] R. K. Nesbet, Phys. Rev. A **20**, 58 (1979).

[40] D. F. Register, S. Trajmar, and S. K. Srivastava, Phys. Rev. A **21**, 1134 (1980).

[41] MKS, Granville-Phillips Division, 6450 Dry Creek Parkway, Longmont, CO 80503 USA.

[42] M. G. P. Homem, I. Iga, R. T. Sugohara, I. P. Sanches, and M.-T. Lee, Rev. Sci. Instrum. **82**, 013109 (2011).

[43] T. W. Shyn and G. R. Carignan, Phys. Rev. A **22**, 923 (1980).

[44] R. D. DuBois and M. E. Rudd, J. Phys. B **9**, 2657 (1976).

[45] R. H. J. Jansen, F. J. de Heer, H. J. Luyken, B. van Wingerden, and H. J. Blaauw, J. Phys. B **9**, 185 (1976).

[46] M. V. Buk, F. P. Bardela, L. A. Silva, I. Iga, and M. G. P. Homem, J. Phys. B: At., Mol. Opt. Phys. **51**, 095201 (2018).

[47] K. Fedus, C. Navarro, L. R. Hargreaves, M. A. Khakoo, F. M. Silva, M. H. F. Bettega, C. Winstead, and V. McKoy, Phys. Rev. A **90**, 032708 (2014).

[48] K. Takatsuka and V. McKoy, Phys. Rev. A **30**, 1734 (1984).

[49] R. F. da Costa, M. T. d. N. Varella, M. H. Bettega, and M. A. Lima, Eur. Phys. J. D **69**, 159 (2015).

[50] *Trichloromethane* (National Institute of Standards and Technology, Gaithersburg, MD, 2018), https://cccbdb.nist.gov/exp2x.asp?casno=67663&charge=0.

[51] G. B. Bachelet, D. R. Hamann, and M. Schlüter, Phys. Rev. B **26**, 4199 (1982).

[52] M. H. F. Bettega, A. P. P. Natalense, M. A. P. Lima, and L. G. Ferreira, Int. J. Quantum Chem. **60**, 821 (1996).

[53] T. H. Dunning, Jr., J. Chem. Phys. **90**, 1007 (1989).

[54] W. J. Hunt and W. A. Goddard, Chem. Phys. Lett. **3**, 414 (1969).

[55] D. Lide, *CRC Handbook of Chemistry and Physics: A Ready-Reference Book of Chemical and Physical Data* (CRC Press, Boca Raton, FL, 1992).

[56] M. de Oliveira, R. F. da Costa, S. A. Sanchez, A. P. P. Natalense, M. H. F. Bettega, and M. A. P. Lima, Phys. Chem. Chem. Phys. **15**, 1682 (2013).

[57] M. T. d. N. Varella, M. H. F. Bettega, M. A. P. Lima, and L. G. Ferreira, J. Chem. Phys. **111**, 6396 (1999).

[58] F. A. Gianturco, R. R. Lucchese, and N. Sanna, J. Chem. Phys. **100**, 6464 (1994).

[59] A. P. P. Natalense and R. R. Lucchese, J. Chem. Phys. **111**, 5344 (1999).

[60] P. Rawat, M. G. P. Homem, R. T. Sugohara, I. P. Sanches, I. Iga, G. L. C. de Souza, A. S. dos Santos, R. R. Lucchese, L. E. Machado, L. M. Brescansin, and M.-T. Lee, J. Phys. B: At., Mol. Opt. Phys. **43**, 225202 (2010).

[61] G. L. C. de Souza, M.-T. Lee, I. P. Sanches, P. Rawat, I. Iga, A. S. dos Santos, L. E. Machado, R. R. Lucchese, L. M. Brescansin, M. G. P. Homem, and R. R. Lucchese, Phys. Rev. A **82**, 012709 (2010).

[62] M.-T. Lee, G. L. C. de Souza, L. E. Machado, L. M. Brescansin, A. S. dos Santos, R. R. Lucchese, R. T. Sugohara, M. G. P. Homem, I. P. Sanches, and I. Iga, J. Chem. Phys. **136**, 114311 (2012).

[63] L. A. da Silva, V. A. S. da Mata, G. L. C. de Souza, I. Iga, L. E. Machado, R. R. Lucchese, M.-T. Lee, and M. G. P. Homem, Phys. Rev. A **94**, 052704 (2016).

[64] J. P. Perdew and A. Zunger, Phys. Rev. B **23**, 5048 (1981).

[65] M.-T. Lee, I. Iga, L. E. Machado, L. M. Brescansin, E. A. y Castro, I. P. Sanches, and G. L. C. de Souza, J. Electron Spectrosc. Relat. Phenom. **155**, 14 (2007).

[66] G. Staszewska, D. W. Schwenke, and D. G. Truhlar, Phys. Rev. A **29**, 3078 (1984).

[67] A. A. Granovsky, Firefly version 8, http://classic.chem.msu.su/gran/firefly/index.html.

[68] M. W. Schmidt, K. K. Baldridge, J. A. Boatz, S. T. Elbert, M. S. Gordon, J. H. Jensen, S. Koseki, N. Matsunaga, K. A. Nguyen, S. Su, T. L. Windus, M. Dupius, and J. A. Montgomery, J. Comput. Chem. **14**, 1347 (1993).

[69] P. G. Burke, N. Chandra, and F. A. Gianturco, J. Phys. B **5**, 2212 (1972).

[70] L. E. Machado, L. Mu-Tao, L. M. Brescansin, M. A. P. Lima, and V. McKoy, J. Phys. B: At., Mol. Opt. Phys. **28**, 467 (1995).

[71] M. G. P. Homem, R. T. Sugohara, I. P. Sanches, M.-T. Lee, and I. Iga, Phys. Rev. A **80**, 032705 (2009).

[72] F. Salvat, J. D. Martínez, R. Mayol, and J. Parellada, Phys. Rev. A **36**, 467 (1987).

[73] J. B. Furness and I. E. McCarthy, J. Phys. B **6**, 2280 (1973).

[74] D. Raj, Phys. Lett. A **160**, 571 (1991).

[75] R. F. da Costa, M. H. F. Bettega, M. A. P. Lima, M. C. A. Lopes, L. R. Hargreaves, G. Serna, and M. A. Khakoo, Phys. Rev. A **85**, 062706 (2012).

[76] K. Aflatooni, G. A. Gallup, and P. D. Burrow, J. Chem. Phys. **132**, 094306 (2010).

[77] P. J. Singh, A. Shastri, R. D'Souza, and B. N. Jagatap, J. Quant. Spectrosc. Radiat. Transfer **129**, 204 (2013).